



This is a repository copy of *Simultaneous thermal and visual imaging of liquid water of the PEM fuel cell flow channels*.

White Rose Research Online URL for this paper:
<http://eprints.whiterose.ac.uk/126795/>

Version: Accepted Version

Article:

Aslam, R.M., Ingham, D.B., Ismail, M.S. et al. (3 more authors) (2019) Simultaneous thermal and visual imaging of liquid water of the PEM fuel cell flow channels. *Journal of the Energy Institute*, 92 (2). pp. 311-318. ISSN 1743-9671

<https://doi.org/10.1016/j.joei.2018.01.005>

Article available under the terms of the CC-BY-NC-ND licence
(<https://creativecommons.org/licenses/by-nc-nd/4.0/>).

Reuse

This article is distributed under the terms of the Creative Commons Attribution-NonCommercial-NoDerivs (CC BY-NC-ND) licence. This licence only allows you to download this work and share it with others as long as you credit the authors, but you can't change the article in any way or use it commercially. More information and the full terms of the licence here: <https://creativecommons.org/licenses/>

Takedown

If you consider content in White Rose Research Online to be in breach of UK law, please notify us by emailing eprints@whiterose.ac.uk including the URL of the record and the reason for the withdrawal request.



eprints@whiterose.ac.uk
<https://eprints.whiterose.ac.uk/>

Title

Simultaneous thermal and visual imaging of liquid water of the PEM fuel cell flow channels

Authors

R. M. Aslam*, D.B. Ingham, M. S. Ismail, K. J. Hughes, L. Ma, M. Pourkashanian

Energy 2050, Department of Mechanical Engineering, Faculty of Engineering, University of Sheffield, Sheffield, S3 7RD, Sheffield. United Kingdom.

*Corresponding author, Tel: +44 114 215 7244

Email address: rmaraaarif1@sheffield.ac.uk (R. M. Aslam)

Abstract

Water flooding and membrane dry-out are two major issues that could be very detrimental to the performance and/or durability of the proton exchange membrane (PEM) fuel cells. The above two phenomena are well-related to the distributions of and the interaction between water saturation and temperature within the membrane electrode assembly (MEA). To obtain insights on the relation between water saturation and temperature, the distributions of liquid water and temperature within a transparent PEM fuel cell have been imaged using high-resolution digital and thermal cameras. A parametric study, in which the air flow rate has been incrementally changed, has been conducted to explore the viability of the proposed experimental procedure to correlate the relation between the distribution of liquid water and temperature along the MEA of the fuel cell. The results have shown that, for the investigated fuel cell, more liquid water and more uniform temperature distribution along MEA at the cathode side are obtained as the air flow rate decreases. Further, the fuel cell performance was found to increase with decreasing air flow rate. All the above results have been discussed.

Keywords: PEMFC; thermal imaging; water management; wetted ratio; direct visualisation

1. Introduction

Proton exchange membrane (PEM) fuel cells are promising clean energy sources for a wide range of portable, automotive and stationary applications and this is due to their quick start-up and sizing flexibility [1]–[4].

However there are some challenges that need to be resolved in order for the PEM fuel cell technology to be widely commercialized, namely the relatively low durability and water flooding [5]–[7]. The performance of the PEM fuel cell highly relies on how liquid water is managed within the fuel cell. In order to ensure reasonable high ionic conductivity of the membrane, the membrane needs to be adequately hydrated with liquid water [8]. Further, inadequate hydration of the membrane may lead to local dry areas, excessive ohmic heating and, consequently, pinhole formation [9]. Equally, it is important to remove excessive liquid water at the cathode to avoid flooding of the catalyst layer and the gas diffusion layer (GDL) and subsequent reactant starvation [10]. On the other hand, the status (i.e. vapour or liquid) and amount of water is highly affected by temperature as saturation pressure, which is used to determine saturation of water, is a strong function of temperature. The sources of heat in PEM fuel cells are (i) entropic (ii) irreversible due to the voltage losses (i.e. activation, ohmic and concentration losses) and (iii) due to phase change through condensation/evaporation [11]–[13]. Generally, the heat is transported through the cell components through conduction and eventually is removed via the reactant gases in the flow field channels. Because of the strong relation between amount and status of water and temperature, the simultaneous investigation of the distribution of liquid water and temperature will be of great benefit and interest to the designers and modellers of PEM fuel cell. Namely, such investigations will assist in obtaining better understanding on how liquid water is correlated to the distribution of temperature within the fuel cell. Eventually, this will provide insights on how liquid water

and temperature could be both managed to prevent undesirable phenomena of water flooding and membrane dehydration.

There have been numerous investigations in which the temperatures within PEM fuel cells have been measured using thermocouples, micro-sensors and infrared thermal camera; see for example [14]–[18]. However, the studies in which the distributions of liquid water and temperature have been simultaneously investigated are scarce. Hakenjos et al. [19] designed a transparent PEM fuel cell to allow simultaneous investigation of the temperature and water distributions under different air flow rates. They reported that the enthalpy of condensation is the cause for an elevated temperature in areas where liquid water is observed. Kim et al. [20] performed a similar investigation to that of Hakenjos et al. [19] and reached to the same conclusion, i.e. the enthalpy of condensation is the cause for the high temperatures in the areas where liquid water is observed. Both of the above research groups presented the images of the temperature and water distribution at the cathode side from the infrared thermal camera and digital camera, respectively. However, the liquid water at the anode side has not been visualized in the above investigations. The liquid water at the anode side may be a performance-limiting factor as it may cause flooding under certain conditions, e.g. when operating the fuel cell under a low current density or when the humidifying water of the fuel condensates under certain operating conditions [21], [22]. Also, no quantitative indicators of water flooding in the flow channels have been introduced in the above two investigations. To this end, the objective in this paper is to present and discuss an experimental procedure which simultaneously images the distributions of temperature and liquid water at the cathode side and the distribution of liquid water at the anode side. Also, in this work, a quantitative indicator of water flooding, the wetted bend ratio has been introduced and employed to help explain the obtained results. The outline of the paper is as follows. The experimental procedures are described in the following section. The thermal and visual images are

presented and discussed in the Results and Discussion Section. Finally, the main findings are stated in the Conclusions Section. Hence, in this paper, the newly-introduced experimental procedure is present and the quantitative indicator of water flooding; the water bend ratio has been employed [23] to investigate the water and thermal management simultaneously.

2. Experimental Investigation

2.1 Fuel cell test station

A commercial transparent PEM fuel cell, CPK202 ClearPak (Pragma Industries) is used to carry out the experimental technique. Its active area is 25 cm^2 and its flow field is a single-pass serpentine. The current collectors were made from gold plated copper. The electrolyte used is Nafion with a thickness of $25 \text{ }\mu\text{m}$, and the catalyst loading is 0.3 mg Pt/cm^2 at the anode and 0.6 mg Pt/cm^2 at the cathode. The fuel cell was not heated and therefore its temperature was, in general, slightly higher than room temperature, e.g. $22\text{-}24^\circ\text{C}$. An in-house fuel cell test station is used to operate the PEM fuel cell, see Fig. 1, and bubble humidifiers have been installed in the test station. This type of humidifier is characterized by: ease of operation and the small power demand. Nevertheless, the main issue with such humidifiers is that the gas-vapour mixture may condense along the gas tube before entering the fuel cell. Fortunately, this issue could be prevented by making the temperature of the downstream gas tube slightly higher than that of the bubble humidifier. The humidifier is made from stainless steel and has a capacity of 0.5 litre. The range of operation, in terms of temperature and pressure, are 20 to $85 \text{ }^\circ\text{C}$ and 0 to 2.5 barg , respectively. Two backpressure regulators, installed at the outlets gas pipes of the fuel cell, control the pressure at the two compartments of the fuel cell. The flow rates of the reacting gases supplied to the fuel cell are controlled by the mass flow controllers (HFC 202, Teledyne Hasting Instrument) installed in

the upstream section of the fuel cell test station. The performance of the PEM fuel cell, in the form of potentiostatic and polarization curves, was captured using a GAMRY 3000 coupled with a 30k GAMRY booster.

[Insert Fig. 1]

2.2 PEM fuel cell modification

To allow for more accurate thermal imaging of the cathode side of the fuel cell, where most of the heat is generated, the thickness of the two outermost transparent plates has been reduced from 20 to 6 mm using a milling machine; see Fig. 2. The material of the transparent plate is polymethyl methacrylate (PMMA) which has a relatively low thermal conductivity, namely $0.19 \text{ Wm}^{-1}\text{K}^{-1}$ [24]. Therefore, the above thinning of the transparent plates has been necessary in order to minimize the thermal resistance and allow for the surface of the plate to be as reflective and as close as possible to the magnitude and distribution of the temperature of the MEA.

[Insert Fig. 2]

2.3 Visual and thermal imaging

The distribution of temperature at the cathode side and the liquid water at both the cathode and the anode sides have been simultaneously recorded using thermal and digital cameras; see Fig. 3. As mentioned in the introduction, a parameter extracted from the captured images of the flow channels, the wetted bend ratio, has been employed as an indicator of the amount of liquid water present in the flow channels [25]. This parameter, along with the wetted bend ratio [23], will be used to explain the performance and thermal variations of the fuel cell. The wetted bend ratio is simply calculated by counting the number of bends that are occupied by liquid water and then dividing them by the total number of bends, i.e. 20 in our case. On the

other hand, the total length of the water-covered areas of the channel is measured and then dividing it by the entire length of the channel to calculate the wetted area ratio; sees Fig. 4. For simplicity, we consider the bend of the portion of the channel to be wet when there exists a considerable amount of liquid water in these regions.

[Insert Fig. 3 and Fig. 4]

3. Results and discussion

In order to explore the viability of the above-described experimental procedure to correlate the profiles of the liquid water and temperature within PEM fuel cell, a parametric experimental study has been performed. In this study, the air flow rate has been changed to investigate its effect on the distributions of the temperature and liquid water in the investigated PEM fuel cell. The set of flow rates used were: 0.10, 0.15, 0.20 and 0.25 Standard Litre per Minute (SLPM) which represents the stoichiometry ratios from 2, 3, 4 and 5 respectively. The hydrogen flow rate has been kept constant at 0.05 SLPM, which is the theoretical hydrogen flow rate calculated based on a total current of 8 A and stoichiometry ratio of about 1.5. During the experiment, the operating conditions on the temperature, pressure and relative humidity, were kept constant, namely, the gas inlet temperature and pressure on both sides were about 21 °C and 1 barg, respectively. The relative humidity of the gases entering the fuel cell at both sides has been recorded by a humidity sensor (Hyroflex Rotonic, Switzerland) as 80% and the polarization and potentiostatic results have been recorded for each air flow rate. As described in the previous section, the visual imaging of the liquid water and thermal imaging have been performed simultaneously.

Fig. 5 shows the polarization curves for the corresponding cases in which the air flow rate has been changed from 0.10 to 0.25 SLPM. It can be seen that the fuel cell performance, in general, slightly

decreases as the air flow rate increases from 0.10 to 0.25 SLPM and this is most likely due to the decrease in the level of the humidification of the membrane with increasing flow rate. As it can be inferred from the wetted ratio curves shown in Fig. 7, the level of water available at the flow channels decreases as the air flow rate increases, thus potentially decreasing the amount of liquid water required for adequate humidification of the membrane. Also, it should be noted that compared to the results presented that in a previous work [23], the fuel cell performance is low. This could be attributed to the poor contact between the MEA and the current collectors of the fuel cell resulting from the thinning of the transparent plates. To investigate the status of the liquid water in the flow channels, the potentiostatic curves were generated at 0.60V, see Fig. 6. As with the corresponding polarization curves, it can be seen that, after reaching almost the ‘pseudo’ steady-state condition, the best fuel cell performance is when the air flow rate is 0.10 SLPM and it decreases as the air flow rate increases.

[Insert Fig. 5 and Fig. 6]

The wetted bend ratio and wetted area ratio for both sides of the fuel cell have been calculated from the captured images and are plotted in Fig. 8. It can be seen that they both decrease as the air flow rate increases and this is most likely to be due to the increase in the ability to remove liquid water from the flow channel with an increasing air flow rate. The wetted ratio numbers at the cathode are larger than those of the anode and this is most likely to be due to the fact that the hydrogen flow rate has been kept constant, the curves of the wetted ratios at the anode side are similar to those at the cathode side. This could be attributed to the back diffusion of liquid water from the cathode side to the anode side which apparently decreases with increasing air flow rate. This signifies that the wetted ratio numbers at the anode side can also be used to interpret the relationship between the fuel cell performance and the air flow rate.

Fig. 9 shows the thermal images at the cathode side of the fuel cell as the air flow rate

increases from 0.10 to 0.25 SLPM. The gas inlet is at the upper right corner of the thermal image and the gas outlet is at the lower left corner. As it can be seen from the images, the uniformity in the temperature distribution decreases as the air flow rate increases. Specifically, a ‘hot-spot’ at the downstream of the flow channel near the cathode outlet starts to form and become larger and ‘stronger’ as the air flow rate increases. It has been shown earlier in this section that, for the given operating conditions and the investigated fuel cell, the fuel cell performs better as the air flow rate decreases. Therefore, one would expect the heat generation (and subsequently the temperature) will be a maximum for the 0.10 SLPM case. However, this is not the case. This is most likely due to the observation that the amount of liquid water present in the flow channels is the highest and the most uniform in the 0.10 SLPM; see Fig. 7. The thermal conductivity of the liquid water is one order of magnitude higher than that of air [26]. To this end, the more liquid water present at the cathode, the more heat is conducted to the transparent plate and, subsequently, the more uniform is the temperature distribution recorded by the thermal camera.

[Insert Fig. 7, Fig. 8 and Fig. 9]

4. Conclusions

In this paper, a transparent PEM fuel cell has been simultaneously visually and thermally imaged using high-resolution digital and thermal cameras in order to explore the relation between the distributions of both liquid water and temperature. The focus has been at the cathode side as it is the side at which water is produced. To investigate the viability of the proposed experimental procedure, a parametric study, in which the air flow rate has been incrementally changed, has been conducted. The following are the main observations and/or findings:

- The temperature distribution along the MEA at the cathode side becomes more non-uniform as air flow rate increases. This could be attributed to the observation that the liquid water (which has significantly larger thermal conductivity than air) in the cathode flow channels becomes less as the air flow rate increases, thus resulting in less efficient heat dissipation.
- The above findings could be alternatively expressed in more quantitative: the temperature distribution across the MEA becomes less uniform as the wetted ratio number decreases.
- For the given in-house modified transparent fuel cell, the fuel cell performance decreases as the air flow rate increases. This was attributed to the increases in the rate of water removal from the cathode with increasing air flow rate, leading to the availability of less water to adequately humidify the membrane electrolyte.

Acknowledgements

The first author gratefully acknowledges the Malaysia Government through MARA Education Fund, Malaysia for the funding and the technical assistance from Mr. Dmitry Govorukhin.

References

- [1] C. Dyer, "Fuel cells for portable applications," *Fuel Cells Bull.*, no. 42, pp. 9–10, 2002.
- [2] E. Carcadea, H. Ene, D. B. Ingham, R. Lazar, L. Ma, M. Pourkashanian, and I. Stefanescu, "A computational fluid dynamics analysis of a PEM fuel cell system for power generation," *Int. J. Numer. Methods Heat Fluid Flow*, vol. 17, no. 3, pp. 302–312, 2007.
- [3] K. Sopian and W. R. Wan Daud, "Challenges and future developments in proton exchange membrane fuel cells," *Renew. Energy*, vol. 31, no. 5, pp. 719–727, Apr. 2006.
- [4] O. M. Orogbemi, D. B. Ingham, M. S. Ismail, K. J. Hughes, L. Ma, and M. Pourkashanian, "Through-plane gas permeability of gas diffusion layers and microporous layer: Effects of carbon loading and sintering," *J. Energy Inst.*, 2016.
- [5] A. El-kharouf, A. Chandan, M. Hattenberger, and B. G. Pollet, "Proton exchange membrane fuel cell degradation and testing: review," *J. Energy Inst.*, vol. 85, no. 4, pp. 188–200, 2012.
- [6] M. Rosli, D. Borman, D. Ingham, Ismail, L. Ma, and M. Pourkashanian, "Transparent PEM Fuel Cells for Direct Visualization Experiments," *J. Fuel Cell Sci. Technol.*, vol. 7, no. 6, p. 61015, 2010.
- [7] G. Hu, G. Li, Y. Zheng, Z. Zhang, and Y. Xu, "Optimization and parametric analysis of PEMFC based on an agglomerate model for catalyst layer," *J. Energy Inst.*, vol. 87, no. 2, pp. 163–174, 2014.

- [8] M. S. Ismail, D. Borman, T. Damjanovic, D. B. Ingham, and M. Pourkashanian, "On the through-plane permeability of microporous layer-coated gas diffusion layers used in proton exchange membrane fuel cells," *Int. J. Hydrogen Energy*, vol. 36, no. 16, pp. 10392–10402, 2011.
- [9] H. K. Atiyeh, K. Karan, B. Peppley, A. Phoenix, E. Halliop, and J. Pharoah, "Experimental investigation of the role of a microporous layer on the water transport and performance of a PEM fuel cell," *J. Power Sources*, vol. 170, no. 1, pp. 111–121, Jun. 2007.
- [10] O. M. Orogbemi, D. B. Ingham, M. S. Ismail, K. J. Hughes, L. Ma, and M. Pourkashanian, "The effects of the composition of microporous layers on the permeability of gas diffusion layers used in polymer electrolyte fuel cells," *Int. J. Hydrogen Energy*, vol. 41, no. 46, pp. 21345–21351, 2016.
- [11] M. S. Ismail, D. B. Ingham, K. J. Hughes, L. Ma, and M. Pourkashanian, "Thermal modelling of the cathode in air-breathing PEM fuel cells," *Appl. Energy*, vol. 111, pp. 529–537, 2013.
- [12] M. S. Ismail, D. B. Ingham, K. J. Hughes, L. Ma, and M. Pourkashanian, "An efficient mathematical model for air-breathing PEM fuel cells," *Appl. Energy*, vol. 135, pp. 490–503, 2014.
- [13] E. Afshari, M. Ziaei-Rad, and M. M. Dehkordi, "Numerical investigation on a novel zigzag-shaped flow channel design for cooling plates of PEM fuel cells," *J. Energy Inst.*, pp. 1–12, 2016.
- [14] H. Lin, T.-F. Cao, L. Chen, Y.-L. He, and W.-Q. Tao, "In situ measurement of temperature distribution within a single polymer electrolyte membrane fuel cell," *Int.*

- J. Hydrogen Energy, vol. 37, no. 16, pp. 11871–11886, Aug. 2012.
- [15] K. Jiao, I. E. Alaefour, G. Karimi, and X. Li, “Simultaneous measurement of current and temperature distributions in a proton exchange membrane fuel cell during cold start processes,” *Electrochim. Acta*, vol. 56, no. 8, pp. 2967–2982, Mar. 2011.
- [16] G. Zhang, L. Guo, L. Ma, and H. Liu, “Simultaneous measurement of current and temperature distributions in a proton exchange membrane fuel cell,” *J. Power Sources*, vol. 195, no. 11, pp. 3597–3604, 2010.
- [17] H. Guo, M. H. Wang, F. Ye, and C. F. Ma, “Experimental study of temperature distribution on anodic surface of MEA inside a PEMFC with parallel channels flow bed,” *Int. J. Hydrogen Energy*, vol. 37, no. 17, pp. 13155–13160, 2012.
- [18] M. Noorkami, J. B. Robinson, Q. Meyer, O. a. Obeisun, E. S. Fraga, T. Reisch, P. R. Shearing, and D. J. L. Brett, “Effect of temperature uncertainty on polymer electrolyte fuel cell performance,” *Int. J. Hydrogen Energy*, vol. 39, no. 3, pp. 1439–1448, Jan. 2014.
- [19] A. Hakenjos, H. Muentert, U. Wittstadt, and C. Hebling, “A PEM fuel cell for combined measurement of current and temperature distribution, and flow field flooding,” *J. Power Sources*, vol. 131, no. 1–2, pp. 213–216, May 2004.
- [20] H.-S. Kim and K. Min, “An experimental investigation of temperature distribution and flooding phenomena of cathode flow fields in a proton exchange membrane (PEM) fuel cell,” *J. Mech. Sci. Technol.*, vol. 28, no. 9, pp. 3837–3843, 2014.
- [21] J. O’Rourke, M. Ramani, and M. Arca, “In situ detection of anode flooding of a PEM fuel cell,” *Int. J. Hydrogen Energy*, vol. 34, no. 16, pp. 6765–6770, 2009.
- [22] S. Ge and C.-Y. Wang, “Liquid Water Formation and Transport in the PEFC Anode,”

- J. Electrochem. Soc., vol. 154, no. 10, p. B998, 2007.
- [23] R. M. Aslam, D. B. Ingham, M. S. Ismail, K. J. Hughes, L. Ma, and M. Pourkashanian, “Simultaneous direct visualisation of liquid water in the cathode and anode serpentine flow channels of proton exchange membrane (PEM) fuel cells,” J. Energy Inst., pp. 1–14, 2017.
- [24] M. J. Assael, S. Botsios, K. Gialou, and I. N. Metaxa, “Thermal conductivity of polymethyl methacrylate (PMMA) and borosilicate crown glass BK7,” Int. J. Thermophys., vol. 26, no. 5, pp. 1595–1605, 2005.
- [25] I. S. Hussaini and C.-Y. Wang, “Visualization and quantification of cathode channel flooding in PEM fuel cells,” J. Power Sources, vol. 187, no. 2, pp. 444–451, Feb. 2009.
- [26] F. Barbir, *PEM Fuel Cells : Theory and Practice ACADEMIC PRESS*. Elsevier Academic Press, 2005.

Figures Captions

Fig. 1 A photograph of the in-house fuel cell test station.

Fig. 2 PEM fuel cell with reduced in thickness transparent plates.

Fig. 3 Schematic diagram of the experimental setup (top view)

Fig. 4(a) A photograph of the investigated transparent fuel cell showing the number of the total bends, i.e. 20, and (b) an image that shows the wetted areas in the flow channel [23].

Fig. 5 The polarization curves for all the investigated air flow rates.

Fig. 6 The measured current density at 0.60 V as a function of time for all the investigated air flow rates.

Fig. 7 The images taken for the cathode side at 0.60 V for the cases at which the air flow rate has been changed incrementally from 0.10 to 0.25 SLPM.

Fig. 8 The wetted area and bend ratio numbers at 0.6 V for the (a) cathode and (b) anode sides.

Fig. 9 The thermal images taken for the cathode side at 0.6 V for the investigated cases in which the air flow rate has been changed incrementally from 0.10 to 0.25 SLPM.



Fig. 1

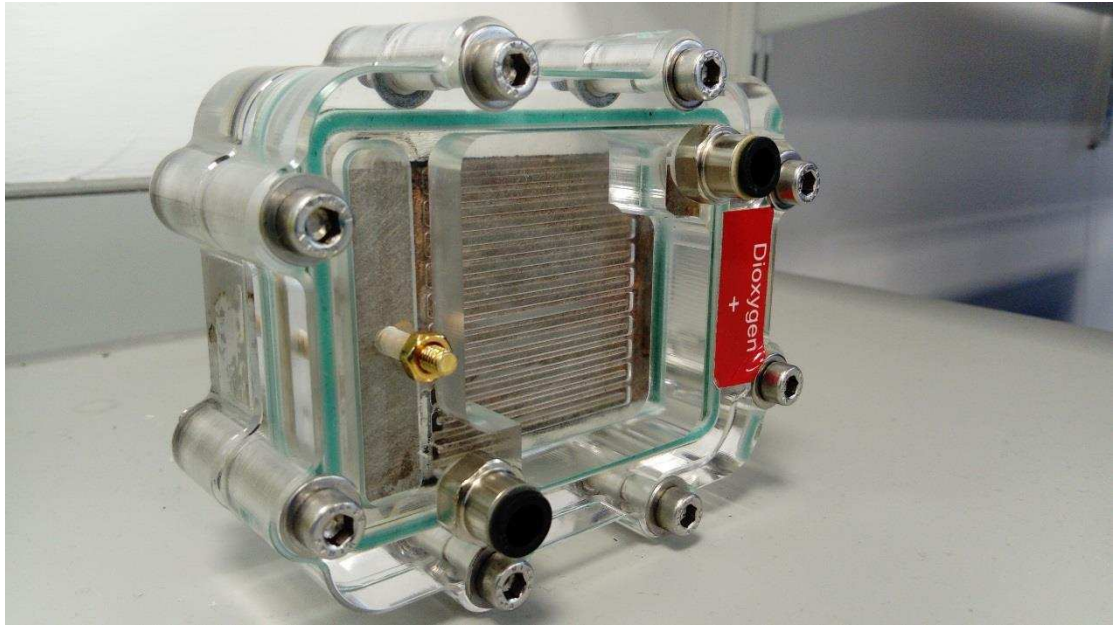


Fig. 2

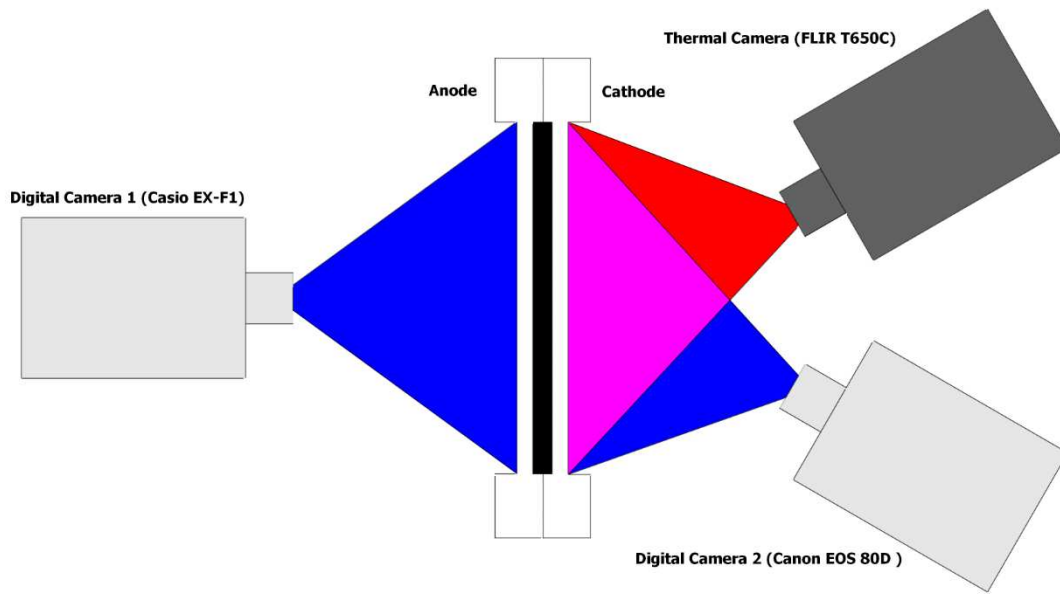


Fig. 3

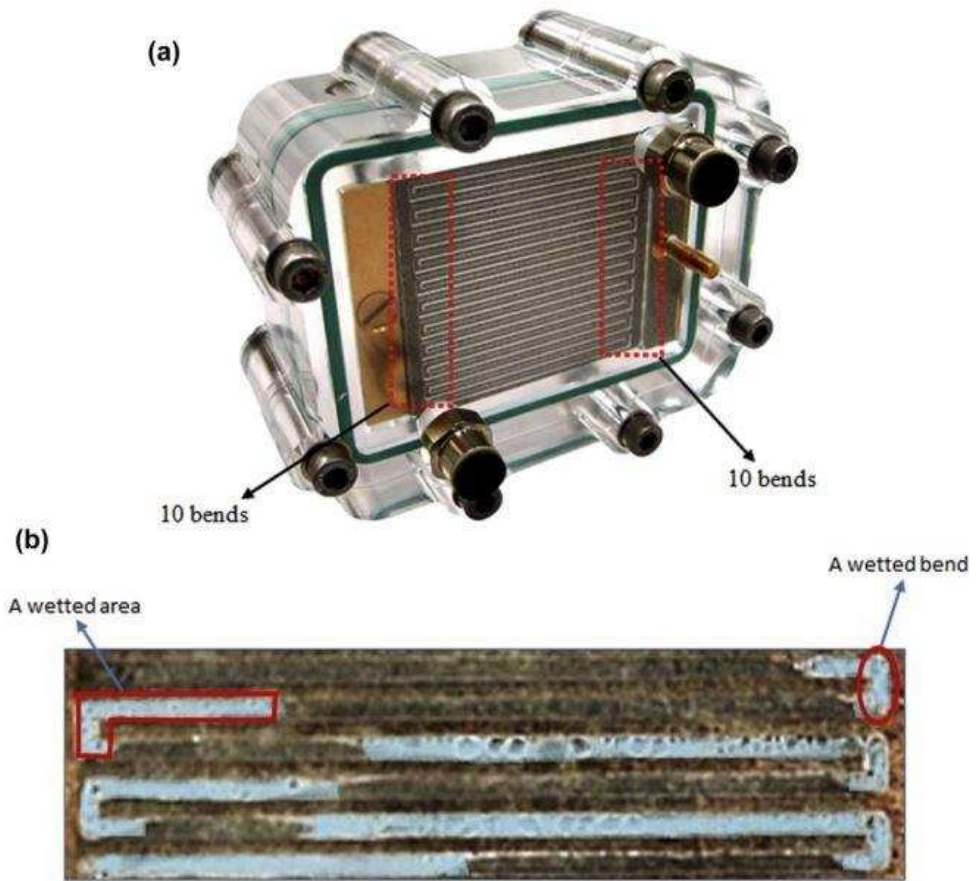


Fig. 4

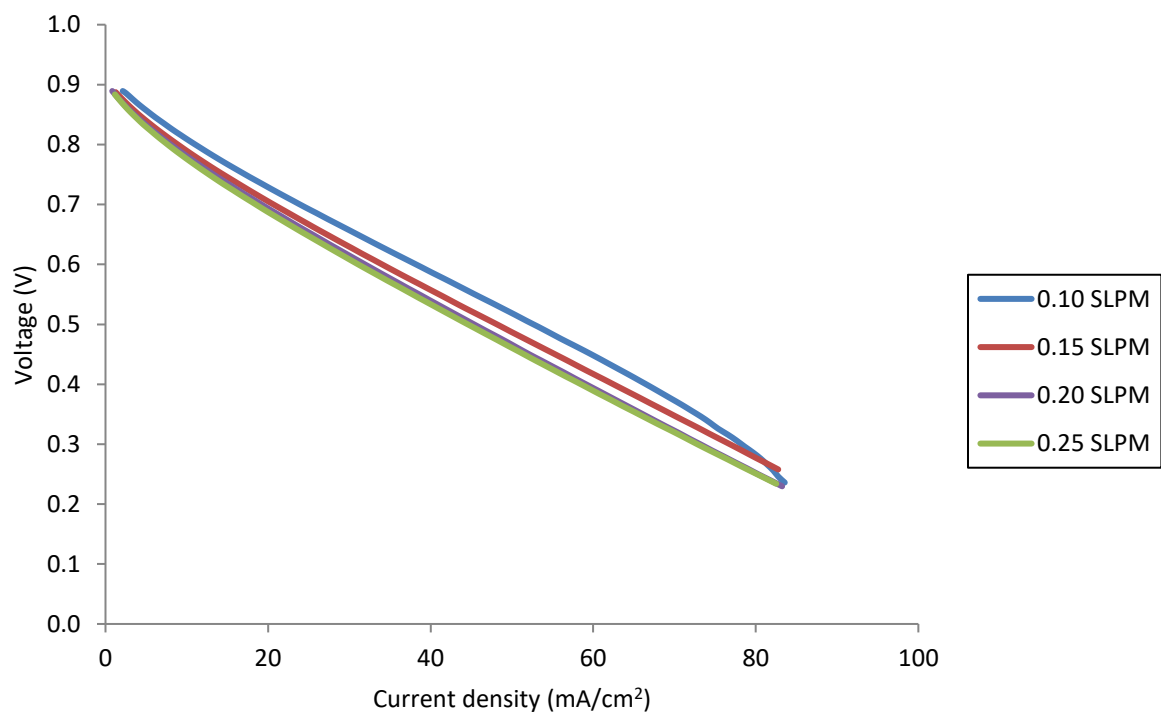


Fig. 5

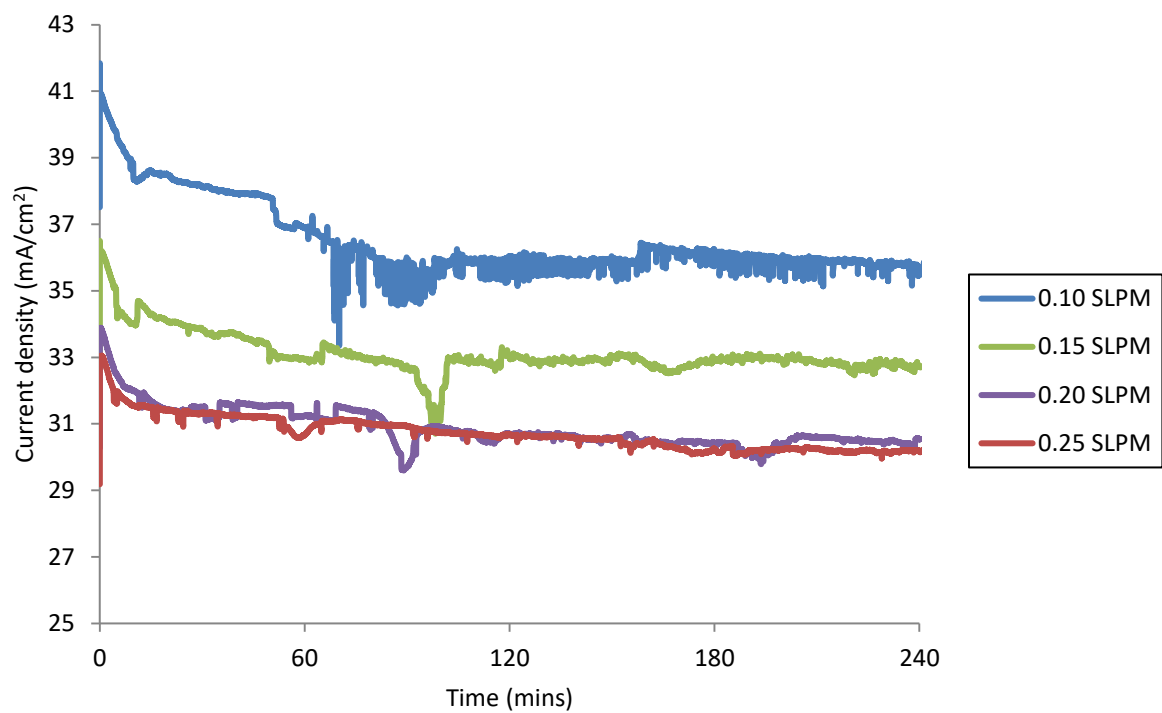


Fig. 6



0.10 SLPM



0.15 SLPM



0.20 SLPM



0.25 SLPM

Fig. 7

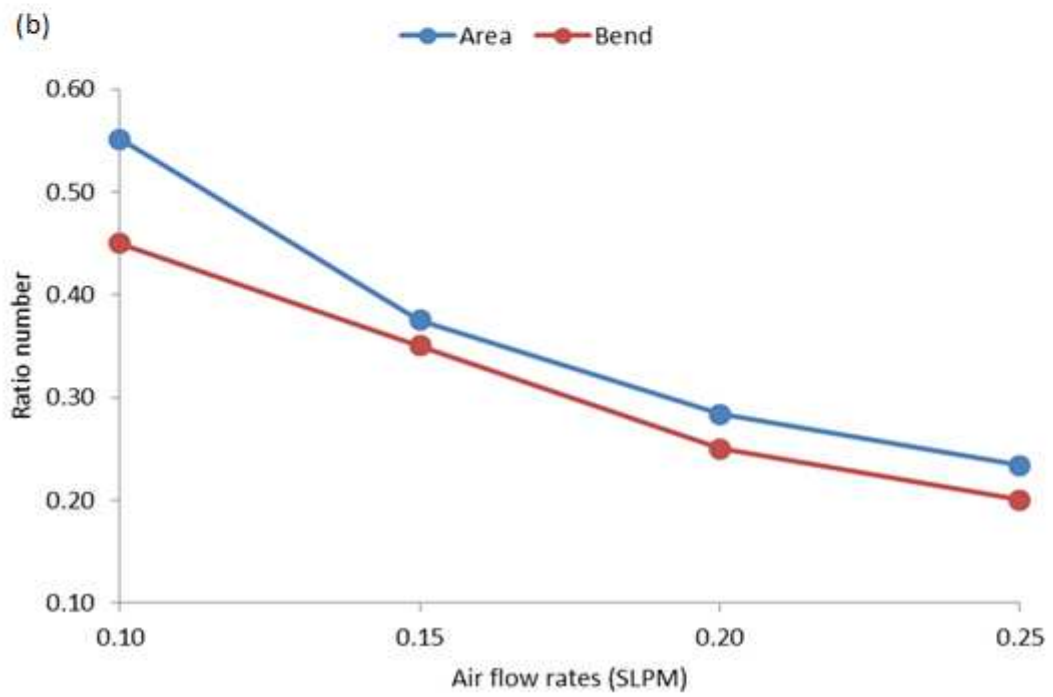
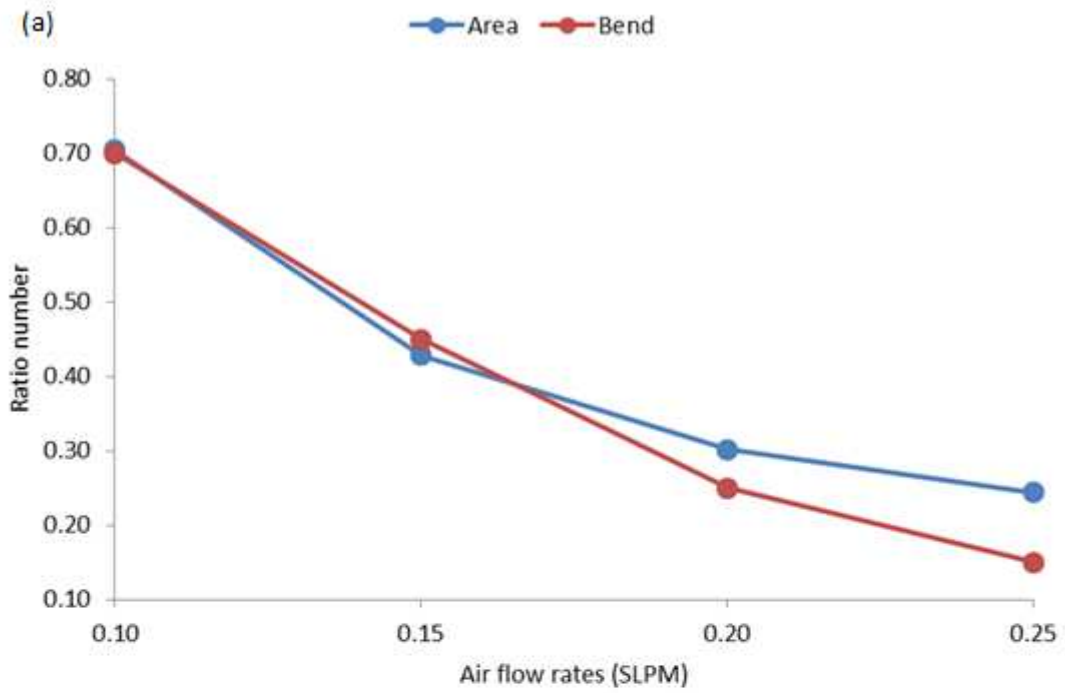


Fig. 8

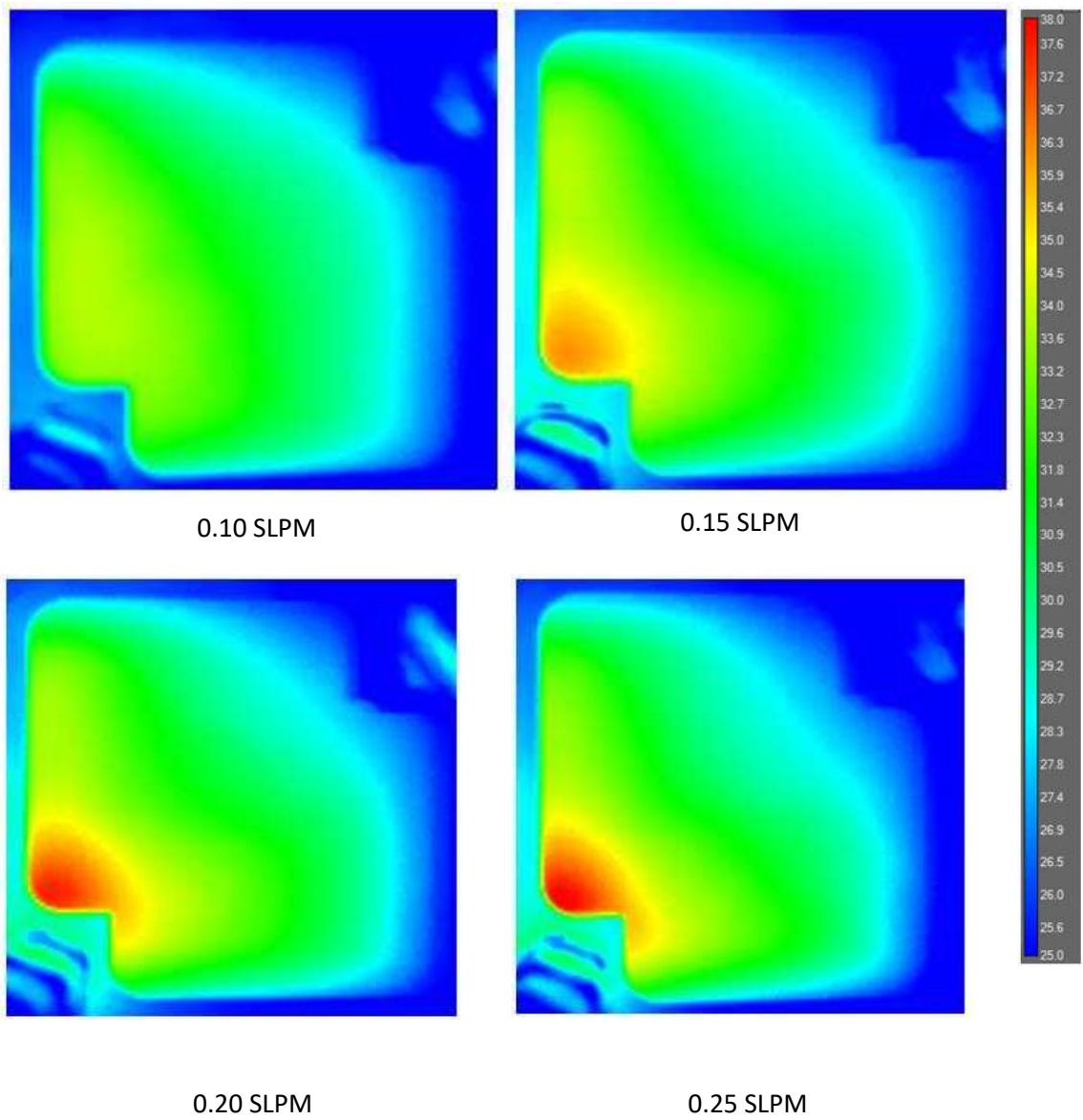


Fig. 9